In-flight Rotor Blade Tip Damage Detection of Small Multirotor using Ultrasonic Sensors

Trans. Japan Soc. Aero. Space Sci.
Vol. 67, No. 4, pp. 203–211, 2024
DOI: 10.2322/tjsass.67.203

In-flight Rotor Blade Tip Damage Detection of Small Multirotor using Ultrasonic Sensors*

Hikaru OTSUKA,[1)†] Akihiro KAWASAKI,[2)] and Hiroshi TOKUTAKE[1)]

[1)]*Faculty of Frontier Engineering, Kanazawa University, Kanazawa, Ishikawa 920–1192, Japan*
[2)]*Graduate School of Natural Science and Technology, Kanazawa University, Kanazawa, Ishikawa 920–1192, Japan*

The prevalence of serious incidents involving small, unmanned multirotors may escalate when such devices are operated within densely populated regions. The development of system fault detection techniques is required to prevent flight-related mishaps. A method utilizing an ultrasonic anemometer to detect damage to the rotor blade tip of a small multirotor has been introduced. This method can detect blade tip damage by analyzing the downwash speed, calculated by incorporating an extended Kalman filter. However, the efficiency of this approach in system fault detection remained ambiguous. To demonstrate the method's feasibility, a comprehensive investigation of rotor downwash was conducted. Employing smoke visualization, hot-wire velocimetry, and ultrasonic anemometry, the mechanics were thoroughly examined. Utilizing the experimental data derived from a quadrotor affixed to a test stand, a novel damage index value was postulated. This index value was then applied in a simulated scenario where one blade tip of a rotor was compromised during hovering flight. The simulation allowed for the detection of a 2-mm blade tip loss on a rotor with a 228.6 mm diameter. This study verified a technique for blade-tip damage detection predicated on sensing wake flow, thereby contributing to multirotor construction with robust failure tolerance mechanisms.

Key Words: Ultrasonic Anemometer, VTOL, Fluid Dynamics, Damage Detection

Nomenclature

J: damage index of rotor blade tip
L: distance between ultrasonic transmitter and receiver
N: number of samples
PSD_1: peak power spectral density of downwash speed at one revolution frequency of rotor
$PSD_{0.5}$: peak power spectral density of downwash speed at half-revolution frequency of rotor
r: horizontal distance from rotor axis
R: rotor radius
T: period of data sampling
t_{dw}: arrival time of ultrasonic wave downward to flow direction
t_{up}: arrival time of ultrasonic wave upward to flow direction
v_d: downwash speed
z: vertical distance from rotor disk plane
θ: inclined angle of ultrasonic sensor path to rotor plane
ψ: rotation phase of rotor blade

*Presented at the 60th Aircraft Symposium, 4–10 October 2022, Niigata, Japan.

Received 14 August 2023; final revision received 20 October 2023; accepted for publication 24 November 2023.

†Corresponding author, h-otsuka@se.kanazawa-u.ac.jp

1. Introduction

Serious incidents may occur more frequently when small unmanned aerial vehicles (UAVs) operate in populated areas. It is thus necessary to analyze the causes of these incidents and construct a robust UAV system for safe UAV flights. Olson and Atkins performed a failure analysis of a small quadrotor and demonstrated the flight failure modes. Further, they proposed several methods to prevent and mitigate failures.[1)] However, during the design phase, there is often a greater emphasis on reducing mass and cost, thereby relegating flight system redundancy to a lesser priority. To achieve a fault-tolerant system without hardware redundancies, it is necessary to accurately identify the predictive signs of failure and reconfigure the control system.

Recently, several studies have performed model-based fault detection of small UAVs. Although the method requires a precise model, additional equipment is not required for fault detection. Asadi, for instance, identified actuator faults in a quadrotor by analyzing the residual values between the predicted sensor output based on the UAV's nominal dynamics model and the actual sensor output.[2)] Similarly, Guo et al. detected sensor faults in small fixed-wing UAVs by comparing the actual sensor output with the estimated sensor output.[3)] Ghalamchi et al. estimated the imbalance of the rotor mass using an accelerometer equipped with a body and a simple kinematic model.[4)] Studies using additional sensors have also been performed for system fault detection. Detection methods using additional sensors can directly identify fault conditions. Altinors et al. utilized a microphone to detect motor and rotor failures using audio data.[5)] Sahwee et al. applied a flexible sensor to the elevator of a fixed-wing UAV to monitor the bending angle and detect elevator faults.[6]

Sensors are also used to monitor rotor wake and can detect damage to a rotor. As for the wake structure, the rotor wake contains blade tip vortices. The vortices caused by the blade tip form a helical structure and move downward along the boundary of the wake flow. Ramasamy et al. visualized isolated rotor wake structures using the laser sheet method.[7] Otsuka et al. visualized quadrotor wake structures in ground effects using particle image velocimetry (PIV).[8] Lee et al. evaluated the downwash velocity (v_d) and wake structure of a small quadrotor using PIV.[9]

The generation of blade-tip vortices causes energy loss during flight. Therefore, commercial small rotor blades are designed to minimize blade tip vortices by twisting the blade or changing the blade tip shape. However, a damaged rotor blade tip generates stronger vortices than a normal blade and changes v_d. Therefore, the blade tip damage can be detected by observing v_d using multirotor sensors.

v_d depends on the blade shape and operating conditions. Thus, precise information on v_d helps understand rotor conditions. Torita et al. constructed an observer system for wind gust disturbances on body angular velocity based on the dynamics of the quadrotor, rotor speed, and body angular velocity. The dynamic model based on blade element and rotor momentum theories contains the parameter v_d of the rotor. They applied a disturbance observer to wind gust response control.[10] Tokutake et al. precisely estimated v_d of a quadrotor using an ultrasonic anemometer.[11] The method for estimating v_d using an ultrasonic anemometer can be used for rotor-fault detection. The system constructed in the study was used to detect blade damage in the present study.

The effect of rotor tip damage on v_d depends on the length of the lost tip part. However, the relationship between blade tip damage and rotor v_d is unclear. Understanding the quadrotor wake with a damaged blade and applying an ultrasonic anemometer to observe the rotor v_d enables the detection of rotor tip damage from the aerodynamic state of the wake. Therefore, the effect of rotor tip damage on the rotor wake velocity must be investigated.

This study aims to demonstrate a system for detecting rotor tip damage of a quadrotor in-flight using an additional sensor, which is an ultrasonic anemometer monitoring rotor wake velocity. First, the wake of a small quadrotor was visualized to clarify the difference in wake structure between damaged and normal rotors. Second, the wake flow speed was measured using the hot-wire method and an ultrasonic anemometer to evaluate v_d change caused by rotor tip damage. The aerodynamic parameters of rotor-tip damage detection using an ultrasonic anemometer were defined from the two experiments. Third, rotor tip damage detection was demonstrated based on the results of ultrasonic anemometer measurements.

The remainder of this paper is organized as follows. Section 2 presents the wake flow visualization of the quadrotor. Section 3 presents the hot-wire velocimetry of a quadrotor wake. Section 4 introduces an algorithm for estimating v_d using an ultrasonic anemometer. Section 5 describes v_d measured by the ultrasonic anemometer; additionally, a parameter for detecting rotor-tip damage is proposed and demonstrated. Finally, Section 6 concludes the paper.

2. Flow Visualization of Damaged Rotor Wake

Flow visualization was conducted to clarify the flow structure of a quadrotor wake with a damaged blade. The quadrotor wake was visualized using the quadrotor model because the wake structure is different between isolated rotor and quadrotor, which causes flow interaction with each other.

2.1. Setup and conditions of the experiment

The experimental quadrotor model is illustrated in Fig. 1. The model is composed of three normal rotors and an evaluation target rotor. The rotors were FC propeller 9045 with a diameter of 228.6 mm, manufactured using nylon. The rotor shaft distance between the rotors in the diagonal position was 450 mm. The quadrotor model was 900 mm above the floor. The rotor height is over seven times the rotor radius. Thus, the ground effect for the rotors is negligible because the rotor thrust does not change when the height is greater than 1.5 times the rotor radius. The rotational speed was controlled using an electric speed controller and a DC brushless motor. The rotational speed of the four rotors was 4800 rpm with a closed-loop control. The rotational directions are shown in Fig. 1. The rotor speed was set such that four rotors could lift a 1.2 kg quadrotor with four rotors.

The evaluation target rotors had four configurations: normal, and chipped at 1, 2, and 10 mm in the flow visualization. Figure 2 shows the experimental target rotors, and Table 1 lists the experimental conditions. Figure 3 shows the exper-

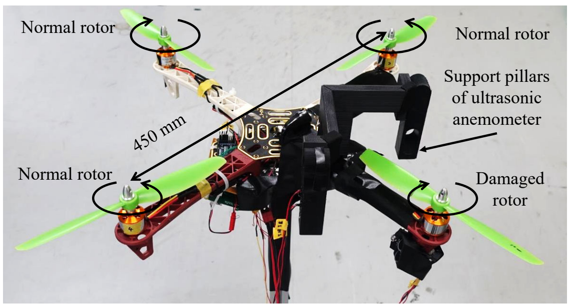

Fig. 1. Quadrotor model used in downwash measurement.

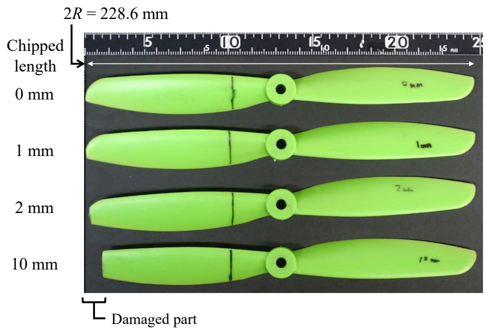

Fig. 2. Experimental target rotors with varied chipped part lengths.

Table 1. Experimental conditions and quadrotor configurations.

Rotor speed	4800	rpm
Rotor diameter	228.6	mm
Distance between adjacent rotors	450	mm
Blade chipped length	0, 1, 2, 10	mm
(Ratio to rotor radius)	(0, 0.9, 1.6, 8.7)	(%)
Rotational direction in top view	Clockwise	

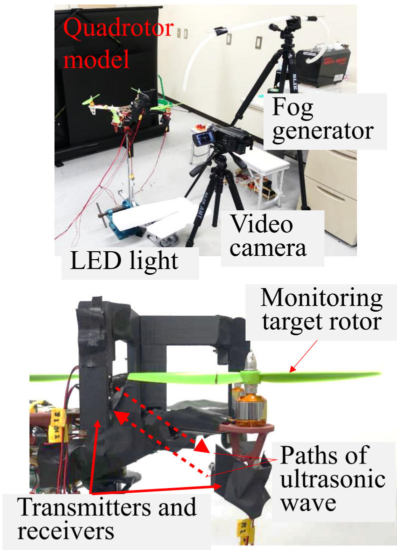

Fig. 3. Setup of flow visualization using smoke.

Table 2. Camera setting in visualization.

Shutter speed	1/1000	s
F-number	2.8	
Camera gain	18	dB
Frame rate	960	fps

imental setup and the paths of the ultrasonic waves. An ultrasonic anemometer was used for velocimetry as described in Section 3. The anemometer measured the average v_d along the path lines.

The rotor wake was visualized using smoke generated with a fog generator (Dainich, Porta Smoke PS-2005). For visualization, smoke was injected onto the rotor at the tip around the transmitter on the upper side to determine the movement of the blade tip vortices. The visualized flow with smoke was illuminated by a light-emitting diode. The flow was subsequently captured by a video camera (Sony HDR-AX700) operating at 960 fps over a span of 1 s. The conditions for the recorded frames are listed in Table 2. The captured frame was processed to magnify its brightness and clarify the positions of the blade tip vortices. The visualization shows the vortex core as a small black point. The wake flow structure can be clarified by tracing the movement of the vortices. Furthermore, the captured frames were sorted in the rotation phase of the rotor blade based on different capture timings. The movement of the vortices from the sorted frames can be understood because the phenomena of the rotor wake are periodic.

2.2. Results

Figures 4(a) and 4(b) show the visualized quadrotor wake, focusing on the blade tip vortices. Figure 4(a) shows the frames captured during the rotation phase (ψ) of the chipped blade at 10° and 190°. Figure 4(b) compares the visualized wake at 275° when the chipped lengths are 1 and 2 mm. Cross marks indicate the centers of the blade tip vortices generated from normal rotors, and plus marks indicate those from damaged rotors. The vertical lines indicate the horizontal position from the rotor center in steps of 10%. The slanted broken line shows a midline between the pair of ultrasonic wave paths in the ultrasonic anemometer measurements. θ is the angle of the line to the plane of the rotor disk.

The visualized flow shows that the blade tip vortices moved downward, passing through the ultrasonic wave paths. When the tip was not chipped, the vortex trajectory crossed the ultrasonic wave path at $r/R = 0.75$. When the tip was chipped (1 mm), the trajectory of the blade tip vortices was almost the same as when it was not chipped.

However, noticeable variations in vortex trajectories were observed between the damaged and the undamaged blades when the chip in the blade length exceeded 1 mm. Vortices originating from the damaged rotor intersected the ultrasonic wave path at $r/R = 0.75$. The vortex trajectory from the normal blade crossed the ultrasonic wave path at $r/R = 0.85$. Flow visualization showed that the black area in the center of the vortices became large when the chipped blade length was greater than 1 mm. It seemed that the vortices from the damaged blade were somewhat stronger compared to those from the normal blade. Blade tip vortices interfere with each other and change the trajectories. Particularly, when the blade damage extended beyond 2 mm, pronounced vortices from the damaged blade seemed to deflect the vortices of the undamaged blade further outwards, leading to bifurcated trajectories.

The velocity difference along the path was predicted from the perspective of v_d on the ultrasonic wave path. With two undamaged blades in operation, a velocity oscillating at 160 Hz is attributed to both the vortex sheet and blade tip vortices passing the trajectory at twice the revolution frequency of the rotor of 4800 rpm. When one blade is chipped, an 80 Hz oscillation in the velocity can be observed according to the rotor revolution frequency. Therefore, observing and analyzing the rotor wake velocity change in the frequency domain can identify blade tip damage during flight.

In Section 3, the state of the wake velocity is evaluated using hot-wire velocimetry to clarify the effect of blade chipping on the rotor wake velocity.

3. Downwash Velocity Measurement using Hot-wire Velocimetry

v_d of rotor was evaluated using hot-wire velocimetry. The primary objective of the experiment was to elucidate the impact of blade tip damage on rotor wake velocity and identify a parameter for detecting such damage by focusing on v_d. The flow visualization showed the difference in the trajectory

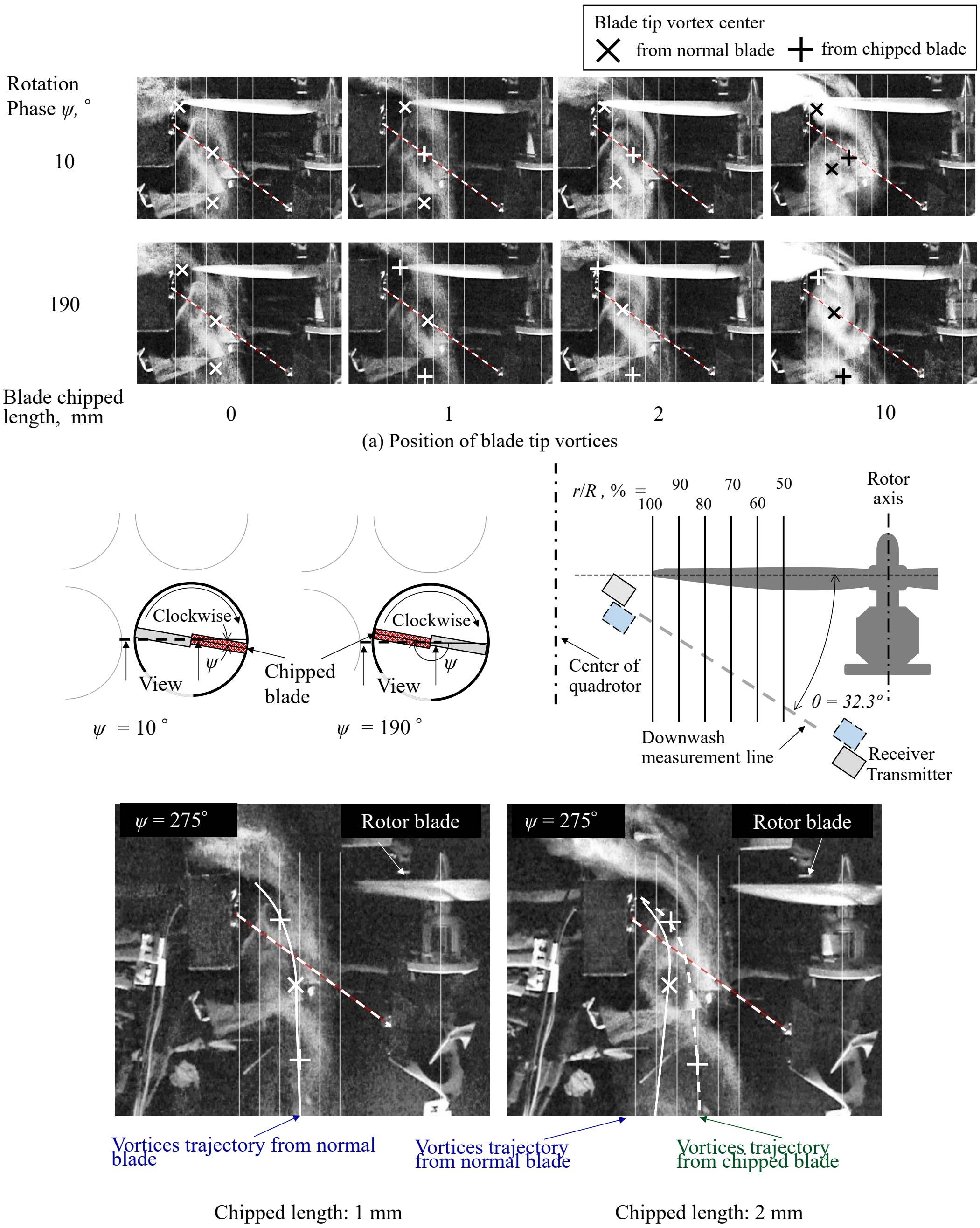

(a) Position of blade tip vortices

(b) Trajectories of blade tip vortices

Fig. 4. Vortices generated from rotor tips in variation of chipped length.

of the blade tip vortices caused by blade chipping. Thus, rotor v_d near the trajectory of the blade tip vortex pass was the focus of this experiment.

3.1. Experimental setup

The quadrotor model and rotor were the same as those used in the flow visualization. We measured v_d at 10 points on the ultrasonic wave path. The positions of v_d measurement are listed in Table 3 and shown in Fig. 5. The measurement points were set on the midline of the two ultrasonic wave paths in Fig. 5(b), which shows the cross section of quadrotor wake (A–A′ plane in Fig. 5(a)) on the measurements point. v_d was measured using hot-wire velocimetry (Kanomax, Smart CTA7250) at these points. The rotation phase for all cases was synchronized in the measurements using a photo reflector. The hot wire velocimetry conditions are listed in Table 4. The measurement frequency was 20 kHz

Table 3. Hot-wire measurement positions.

r/R	0.33	0.41	0.48	0.56	0.63
r, mm	38	47	55	64	72
z, mm	72	66	61	56	51
r/R	0.71	0.78	0.85	0.93	1.00
r, mm	80	89	97	106	114
z, mm	45	40	35	29	24

*$R = 114.3$ mm.

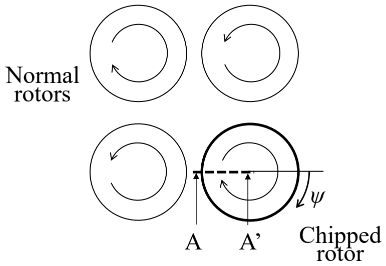

(a) Top view

Position	r mm	z mm
Transmitter 1	125.4	7.8
Receiver 1	24.6	70.2
Transmitter 2	125.4	26.8
Receiver 2	24.6	89.2

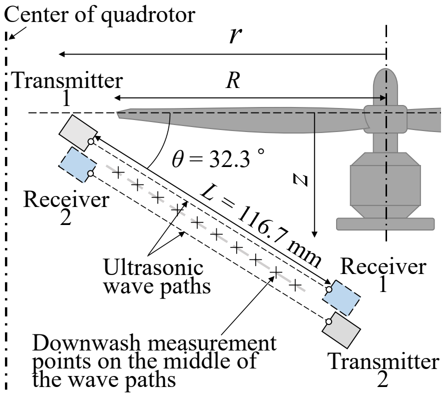

(b) Side view (A–A′)

Fig. 5. Measurement points of v_d using hot-wire velocimetry.

and sampled for 0.5 s. The hot-wire probe was calibrated at 0, 7, and 14 m/s using a small wind tunnel. The measured v_d at each point was recorded using a data logger, and the power spectrum density (PSD) in the frequency domain was analyzed.

3.2. Results and discussion

Figure 6(a) shows the average v_d and the standard deviation (SD) of v_d at the measurement positions. The points show the average velocity, and the error bars show the standard deviation. Figure 6(b) shows the downwash velocity at $r/R = 0.78$, 0.85, and 0.93 in the time domain. Figure 7 shows the power spectral density (PSD) of the downwash speed in the frequency domain at $r/R = 0.78$, 0.85, and 0.93. In the experiment, the SD and PSD were calculated using the following equations:

$$SD = \sqrt{\frac{1}{N}\sum_{i=1}^{N}(v_{di} - \hat{v}_{di})^2}, \tag{1}$$

$$\hat{v}_{di} = \frac{1}{N}\sum_{i=1}^{N} v_{di}, \tag{2}$$

$$PSD(f) = \lim_{T\to\infty}\frac{|v_d(f)|^2}{T}, \tag{3}$$

Table 4. Conditions of hot-wire anemometry.

Sampling rate	20 kHz
Probe	Tungsten wire X-type probe
Method	Constant temperature anemometry
Calibration speed range	0–14 m/s

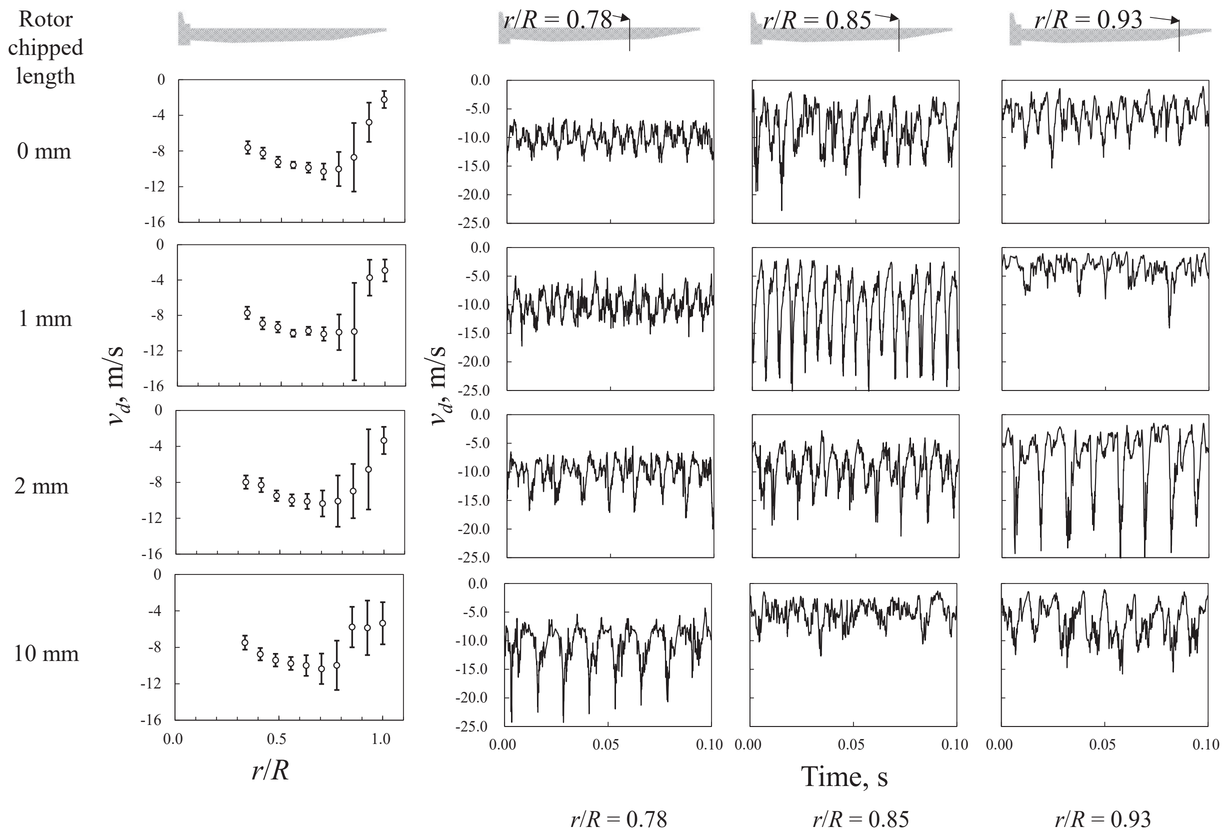

(a) Averaged v_d

(b) History of v_d

Fig. 6. V_d distribution under rotor in hot-wire velocimetry.

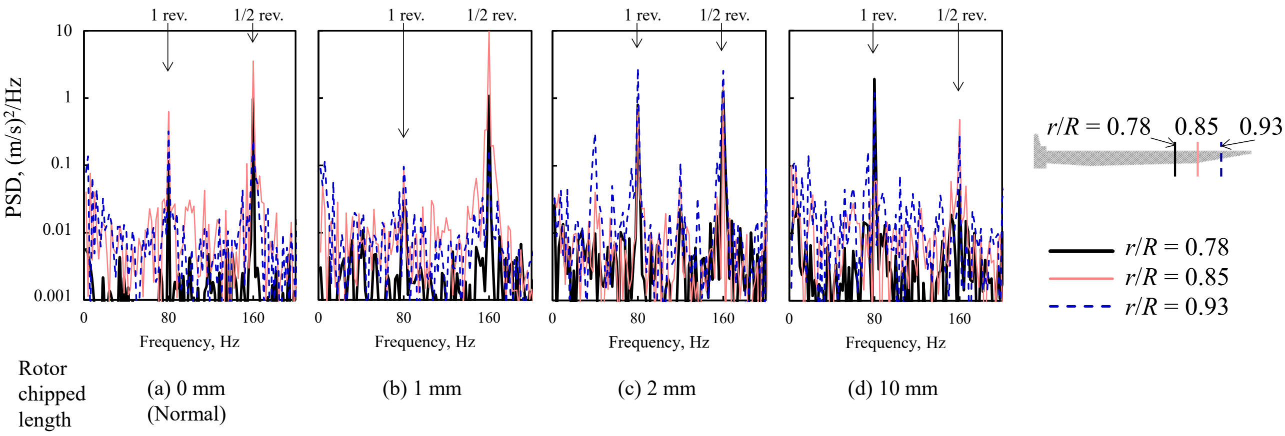

Fig. 7. Power spectral density of v_d in frequency domain measured using hot-wire velocimetry.

where number of samples N was 10000; v_{di} is the downwash speed at sampling timing, $v_d(f)$ is Fourier transform of v_d, and T is the sampling time period between the start and end of PSD calculations (0.5 s).

When the blade chipped length was smaller than 2 mm, a significant oscillation of v_d was observed at $r/R = 0.85$ (Fig. 6(a)). Under the conditions studied, an oscillation was discerned with a period of 6.25 ms (160 Hz) (as depicted in Fig. 6(b)). Notably, this frequency corresponds with the path passage of the vortices originating from the undamaged blades.

When the chipped length was the same as or greater than 2 mm, the downwash speed oscillation was significant at $r/R = 0.78$ and 0.93 (Fig. 6(a)). The oscillation frequency was 80 Hz, which coincided with the frequency of the vortices passing through the path from the damaged blade.

As the blade chipped length increased from 1 to 2 mm, the SD of v_d increased at $r/R = 0.71$, 0.78, and 0.93 (Fig. 6(a)). In contrast, the SD of v_d decreased at $r/R = 0.85$.

In Fig. 7, a peak PSD is observed at 80 Hz and 160 Hz under the experimental conditions. The 160 Hz frequency coincided with the frequency of the rotor blade passing at 4800 rpm with two blades. The PSD peak occurred at 160 Hz when the chipped length was 0 or 1 mm. When the chipped length was equal to or greater than 2 mm, the PSD peak shifted from 160 to 80 Hz. When the blade chipped length was less than 2 mm, the blade tip vortices passed the measurement points at the same position along the trajectory, as shown in the flow visualization. Thus, the downwash speed oscillation was observed at the same point with the same frequency of 160 Hz.

The hot-wire velocimetry results agreed with the flow visualization results and showed v_d oscillation of 160 Hz when the chipped length was 0 or 1 mm. The flow visualization results explained the shift of the v_d oscillation peak from 160 to 80 Hz. When the chipped length was greater than 1 mm, the trajectory of the blade tip vortices from the damaged and normal blades broke into two in the visualization. Therefore, the downwash speed oscillation was significant at two of the measurement points, and the oscillation frequency shifted from 160 to 80 Hz because the vortex trajectories crossed at different points.

From the perspective of damage detection at the blade tip, blade chipping can be detected by observing the shifting power spectral density at the downwash speed in the frequency domain.

Therefore, it is assumed that setting the threshold at the power deviation in the averaged downwash speed indicates blade damage over a 1 mm chipping. In particular, the power deviation at the rotor revolution frequency is appropriate for observing blade tip damage.

Although hot-wire velocimetry detected blade tip damage, the validity of downwash measurements using ultrasonic sensors is unclear. In hot-wire velocimetry, the flow speed is noted at specific points. An ultrasonic anemometer measures the average v_d on the path, in contrast to hot-wire velocimetry, which measures specific points on the path. Therefore, the feasibility of using an ultrasonic anemometer for blade damage detection will be clarified and discussed in Sections 4 and 5.

4. Method of Downwash Speed Estimation using an Ultrasonic Anemometer

In this section, the downwash estimation method is briefly described. The detailed measurement process has been described in a previous study.[11)] The waveform propagates between the transmitter and receiver set under the rotor. The wave travels along the path at a speed that is the sum of the sonic speed and v_d component linear to the path. Therefore, the rotor v_d can be estimated from the traveling time of the ultrasonic wave along the path below the rotor. The ultrasonic anemometer comprised two pairs of ultrasonic transmitters and receivers arranged under the rotor (Fig. 5). v_d was calculated from the time of the upward and downward paths of the ultrasonic wave as follows:

$$v_d = \frac{L}{2\sin\theta}\left(\frac{1}{t_{dw}} - \frac{1}{t_{up}}\right), \tag{4}$$

where t_{dw} and t_{up} are the times required for the downward and upward travel, respectively. L is the length of the ultrasonic wave paths in the downwash. In Eq. (4), v_d does not

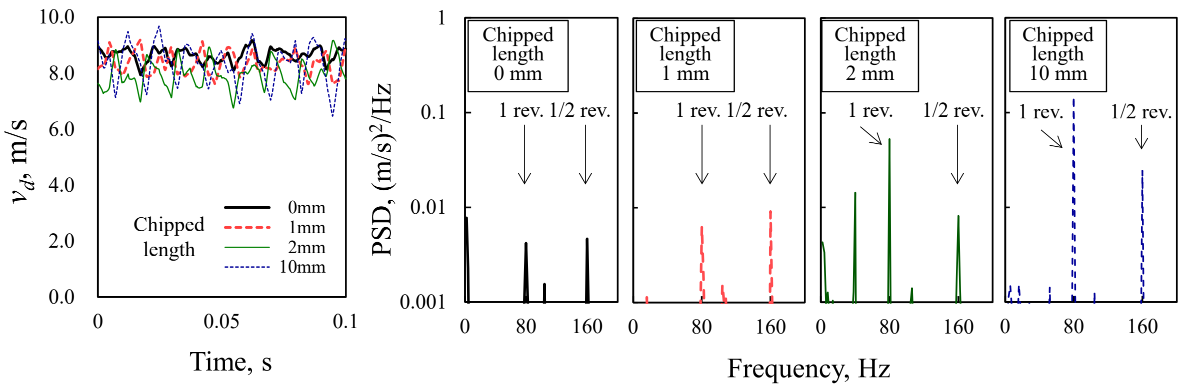

(a) v_d

(b) PSD of v_d

Fig. 8. Estimated averaged v_d on wave path using ultrasonic anemometer and power spectrum density in frequency domain.

depend on the sonic speed when calculated using t_{dw} and t_{up}. This formulation assumes that v_d is constant on the ultrasonic wave paths and that the vertical component of the velocity is dominant in the downwash. It should be noted that the amplitude and waveform of the received ultrasonic wave varied because of the passing distance and disturbed downwash. The passing time can be estimated by applying an extended Kalman filter with the ultrasonic transmitter and the receiver outputs, the same as in a previous work.[11)]

5. Rotor Damage Detection using an Ultrasonic Anemometer

In Section 3, we verified that the rotor downwash velocity distribution undergoes alterations owing to damage at the blade tip of the rotor blade. In this section, downwash estimation using an ultrasonic anemometer is presented, and a method to detect blade tip damage is proposed. The feasibility of this method is examined using simulations.

5.1. Downwash speed estimation

5.1.1. Experiment setup and condition

The rotor downwash speed was estimated using an ultrasonic anemometer for the variation of chipping damage. The evaluation target rotor was chipped 1, 2, 3, 5, and 10 mm on one side. V_d was observed using an ultrasonic anemometer. Two pairs of ultrasonic transmitters and receivers were arranged below the rotor. In the experiment, the sensors were isolated from the quadrotor model to avoid the effects of quadrotor vibration. The ultrasonic wave paths were inclined toward the rotor plane to measure the components of v_d linear to the paths. The downwash speed was calculated from the difference in arrival times between the two pairs of sensors. The length of the path travelled by the wave (L) was 116.7 mm. Receivers measured the ultrasonic wave at 500 kHz for 0.5 s. Measured data from the two pairs of sensors were recorded with a data logger and processed using a computer, which was not an onboard system. The rotor speed was 4800 rpm, which was the same as that in the hot-wire velocimetry.

5.1.2. Results

The measured v_d values when the blade was chipped 0, 1, 2, and 10 mm using the ultrasonic anemometer are shown in Fig. 8(a). The PSD of the estimated downwash speed is shown in Fig. 8(b).

v_d oscillates at one and two times the rotor revolution frequencies at 80 and 160 Hz, respectively. The oscillation amplitude of the damaged rotor exceeded that of the normal rotor (Fig. 8(a)). The PSD of v_d indicated that the dominant oscillation frequency was 80 Hz when the chipped length was greater than 1 mm and that the peak value of the PSD at 80 Hz increased as the chipped length increased (Fig. 8(b)). The dominant oscillation frequency coincides with the revolution frequency of the damaged blade. The results of the measured v_d imply that the ultrasonic anemometer can detect rotor tip damage similarly to hot-wire velocimetry, as discussed in Section 4.

5.2. Rotor damage detection index

It was verified that v_d measured using an ultrasonic anemometer was sensitive to blade-tip damage and v_d could be used to detect the blade-tip damage. In this study, we propose a method for detecting blade-tip damage by monitoring the ratio of PSD of v_d at 1 and 0.5 revolution frequencies.

The blade-tip damage index J is defined and verified for the damage detection of the rotor blade as follows:

$$J = 10\log_{10}\left(\frac{PSD_1}{PSD_{0.5}}\right) \tag{5}$$

where PSD_1 is the PSD at revolution frequency (80 Hz), and $PSD_{0.5}$ is the half-revolution frequency (160 Hz). The PSD of v_d was calculated from the measured v_d with $N = 400$. The sampling frequency was reduced from 20 kHz to 4 kHz to minimize computational cost. Therefore, T was 0.1 s, which corresponds to a period of eight revolutions of the rotor. The PSD peak frequencies can shift within 2 Hz in fast Fourier transform analyses. Thus, local PSD peaks were searched around 80 and 160 Hz in the calculation process for evaluating J.

Figure 9 shows the time history of J evaluated from measured V_d using the ultrasonic sensor, when rotor was chipped 1, 2, 3, 5, and 10 mm on one side. It can be observed that J of a damaged rotor larger than 1 mm is larger than that of a normal rotor. J values of the normal and 1 mm chipped rotor

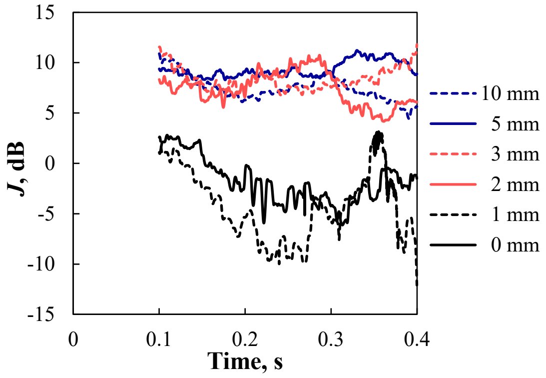

Fig. 9. Time histories of rotor blade-tip damage index J for variation in blade chipped length.

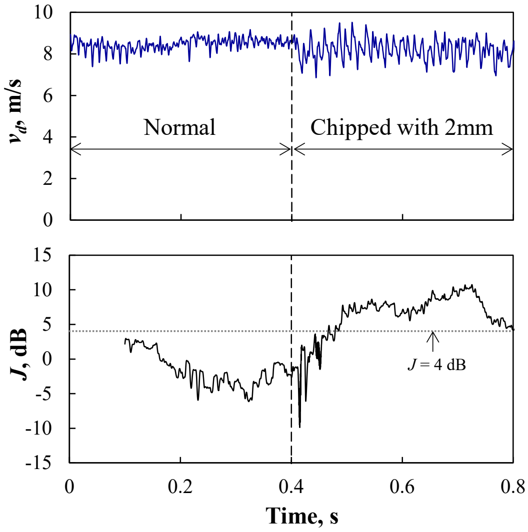

Fig. 10. Simulated J for blade chipped 2 mm during hovering flight.

were below 5. When the chipped length was larger than 1 mm, J ranged from 4 to 14 and was over 5 at most of the measurement timings. Therefore, J can be used to detect blade-tip damage by adopting a threshold value.

5.3. Simulation of rotor tip damage detection according to scenario

The damage-detection method was subsequently applied to a rotor displaying signs of damage, and the effectiveness of this approach was systematically evaluated. To demonstrate the feasibility of the proposed method, damage detection using threshold values was studied by assuming a scenario.

In this scenario, the blade lost a tip of 2 mm during hovering flight, and a chipping event occurred at 0.4 s. The downwash speed estimation method was applied to damage scenario data, and the proposed damage index J was simulated. The data was composed of v_d without blade damage for 0.4 s and with 2 mm chipped damage for 0.4 s, which was measured using the ultrasonic anemometer. J was calculated from the last 0.1 s and appeared from 0.1 s in the simulation.

In this case, Fig. 10 shows the change in J, which increased from under 2.5 to over 4.0 dB after the damage occurred at 0.4 s. The 2 mm chipped damage can be detected by applying a threshold value of approximately 4.0 dB. The proposed method detected a damage size of 2 mm, which was 0.9% of the rotor diameter. The rise time of damage index reacting to rotor damage was approximately 0.08 s, sufficiently faster than airplane dynamics. Consequently, the proposed method has sufficient sensitivity for detecting small damage. The response is sufficiently fast for application to the fault-tolerant control of a multirotor airplane recovering from disturbed dynamics.

Although it was expected that the threshold value of J would depend on the rotor diameter and revolution speed, the simulation results demonstrated the feasibility of the method for detecting rotor tip damage using downwash monitoring with an ultrasonic anemometer. It is worth highlighting that this method distinguishes itself from prevailing alternatives by virtue of its monitoring focus. While most existing methodologies concentrate on monitoring rotor vibrations, accelerometer outputs, angle of elevators or auditory signals emanating from the rotor,[3–6] this particular technique emphasizes the monitoring of flow state. Consequently, it introduces a unique perspective to the field of rotor analysis and damage detection.

Calculation cost reduction and arrangement of appropriate sensor positions are topics for future research. To validate the method for small multirotors, the calculation cost was reduced to estimate the v_d required for the onboard system because our method uses an extended Kalman filter. The sensitivity of the downwash estimation depends on the positions of the transmitters and receivers and the inclined angle of the ultrasonic wave paths. Increasing the angle can enhance the estimation accuracy. The arrangement of the ultrasonic receiver and transmitter is related to the trade-off problems between accurate downwash estimation and minimization of the system weight. Although this study focuses on hovering multirotors, consideration of wake structure changes in forward flights is required.

6. Conclusions

The wake flow of a quadrotor with a damaged rotor blade was visualized, and the downwash speed was measured using hot-wire velocimetry and an ultrasonic anemometer. Based on the experiments, a method was proposed to detect blade tip damage by monitoring the power spectrum density of the downwash speed using an ultrasonic anemometer.

Flow visualization showed that the trajectory of the blade tip vortices depended on the length of the chipped part because the vortex trajectory from the normal blade was moved to the outer side of the rotor by vortices from the damaged blade. Hence, the downwash speed distribution changed periodically with the rotor revolution frequency when the rotor tip was damaged by >1 mm.

Based on the experimental results, an index value J was proposed to detect blade tip damage based on the PSD of v_d

at one and one-half revolution frequencies, and the damage was detected using an ultrasonic anemometer. This method can detect a 0.9% loss of the rotor blade tip by employing an appropriate threshold value in hovering condition in a simulation scenario. The technique to detect blade tip damage in hovering flight by sensing wake flow was verified, which contributes to the construction of a robust multirotor control system.

The crosswind and flight speed affect the downwash speed distribution, and the threshold value was set to reflect the flight conditions. Future tasks include detecting rotor blade tip damage using an ultrasonic anemometer under a wide range of flight conditions.

Acknowledgments

This study was supported by the JSPS KAKENHI (Grant number: JP20K04918). We thank Soshi Okada for supporting our experiments.

References

1) Olson, I. J. and Atkins, E. M.: Qualitative Failure Analysis for a Small Quadrotor Unmanned Aircraft System, AIAA Paper 2013-4761, 2013.
2) Asadi, D.: Model-based Fault Detection and Identification of a Quadrotor with Rotor Fault, *Int. J. Aeronaut. Sp. Sci.*, **23** (2022), pp. 916–928.
3) Guo, D., Wang, Y., Zhong, M., and Zhao, Y.: Fault Detection and Isolation for Unmanned Aerial Vehicle Sensors by Using Extended PMI Filter, *IFAC-PapersOnLine*, **51** (2018), pp. 818–823.
4) Ghalamchi, B., Jia, Z., and Mueller, M. W.: Real-Time Vibration-Based Propeller Fault Diagnosis for Multicopters, *IEEE/ASME Trans. Mechatron.*, **25** (2020), pp. 395–405.
5) Altinors, A., Yol, F., and Yaman, O.: A Sound Based Method for Fault Detection with Statistical Feature Extraction in UAV Motors, *Appl. Acoust.*, **183** (2021), 108325.
6) Sahwee, Z., Rahman, N. A., and Sahari, K. S. M.: Experimental Evaluation of Data Fusion Algorithm for Residual Generation in Detecting UAV Servo Actuator Fault, *Int. J. Micro Air Veh.*, **7** (2015), pp. 133–145.
7) Ramasamy, M., Lee, T. E., and Leishman, J. G.: Flowfield of a Rotating-Wing Micro Air Vehicle, *J. Aircraft*, **44** (2007), pp. 1236–1244.
8) Otsuka, H. and Nagatani, K.: Flow Visualization of Wake of a Quadcopter in Ground Effect, 6th Asian/Australian Rotorcraft Forum and Heli Japan 2017, ARF6-039, 2017.
9) Lee, S., Chae, S., Woo, S. Y., Jang, J., and Kim, J.: Effects of Rotor-Rotor Interaction on the Wake Structure and Thrust Generation of a Quadrotor Unmanned Aerial Vehicle, *IEEE Access*, **9** (2021), pp. 85995–86016.
10) Torita, R., Kishi, T., Tokutake, H., Sunada, S., Tanabe, Y., and Yonezawa, K.: Modeling of Aerodynamic Characteristics of Drone and Improvement of Gust Response, 6th Asian/Australian Rotorcraft Forum and Heli Japan 2017, ARF6-015, 2017.
11) Tokutake, H., Okada, S., Sunada, S., Tanabe, Y., and Yonezawa, K.: On-board Downwash Speed Estimation of Drone Rotor-Based State Observer, *Trans. Jpn. Soc. Aeronaut. Space Sci.*, **65** (2022), pp. 231–236.

Yasutada Tanabe
Associate Editor